J|A|C|S
ARTICLES
Published on Web 03/10/2006

Site-Directed Parallel Spin-Labeling and Paramagnetic Relaxation Enhancement in Structure Determination of Membrane Proteins by Solution NMR Spectroscopy

Binyong Liang, John H. Bushweller, and Lukas K. Tamm*

Contribution from the Department of Molecular Physiology and Biological Physics, University of Virginia, Charlottesville, Virginia 22908-0736

Received November 11, 2005; E-mail: lkt2e@virginia.edu

Abstract: A major challenge for the structure determination of integral membrane proteins by solution NMR spectroscopy is the limited number of NOE restraints in these systems stemming from extensive deuteration. Paramagnetic relaxation enhancement (PRE) by means of nitroxide spin-labels can provide valuable long-range distance information but, in practice, has limits in its application to membrane proteins because spin-labels are often incompletely reduced in highly apolar environments. Using the integral membrane protein OmpA as a model system, we introduce a method of parallel spin-labeling with paramagnetic and diamagnetic labels and show that distances in the range 15−24 Å can be readily determined. The protein was labeled at 11 water-exposed and lipid-covered sites, and 320 PRE distance restraints were measured. The addition of these restraints resulted in significant improvement of the calculated backbone structure of OmpA. Structures of reasonable quality can even be calculated with PRE distance restraints only, i.e., in the absence of NOE distance restraints.

Introduction

Integral membrane proteins constitute approximately one-third of all proteins encoded by the genomes of prokaryotic and eukaryotic cells, where they fulfill numerous important transport, sensing, and signal transduction functions. Membrane proteins continue to be a challenge for structural biology although recent successes bode well for future progress.[1] Recently, the structures of several small (∼20 kDa) β-barrel membrane proteins in detergent micelle complexes (∼50 kDa) have been solved by solution nuclear magnetic resonance (NMR) spectroscopy,[2−5] demonstrating the utility of solution NMR for this class of proteins. Success in this area requires the use of transverse relaxation optimized spectroscopy (TROSY)[6] at high magnetic fields to improve ^{15}N relaxation and extensive deuteration to improve ^{13}C relaxation. The trimeric α-helical membrane protein diacylglycerol kinase with 3 transmembrane (TM) helices and one interfacial helix has also been nearly fully assigned using high-field heteronuclear NMR techniques.[7] High levels of deuteration that are routinely used in these studies result in limited numbers of nuclear Overhauser effect (NOE) data yielding structures of only intermediate quality. The lack of long-range NOEs is exacerbated in the α-helical membrane proteins, where few if any long-range NH−NH NOEs can be obtained, making it difficult to determine the overall fold of the protein. In at least one case, reintroduction of side chain methyl protons in Val, Leu, and Ile has improved the number of long-range NOEs and the structure precision.[4] However, it is not clear how generally useful this approach will be as a majority of these amino acids face the lipid rather than the interior of the protein, resulting in only a limited number of additional long-range NOEs.

Paramagnetic relaxation enhancement (PRE) has long been recognized as a method for providing long-range distance information that can complement NOE restraints, which are limited to distances of up to ∼6 Å.[8] Until recently, the PRE method has not been frequently used because of a lack of suitable paramagnetic centers in proteins. Site-directed spin labeling (SDSL) offers a straightforward approach to introduce paramagnetic nitroxide centers into proteins.[9] Distances from the introduced unpaired electron of the nitroxide to the affected nuclei can be readily calculated from the measured PREs. This approach has been successful in defining the global fold of soluble proteins with limited NOE data.[10−13] Recently, this approach has also been used for the purported integral membrane

(1) Arora, A.; Tamm, L. K. *Curr. Opin. Struct. Biol.* **2001**, *11*, 540−547.
(2) Arora, A.; Abildgaard, F.; Bushweller, J. H.; Tamm, L. K. *Nat. Struct. Biol.* **2001**, *8*, 334−338.
(3) Fernández, C.; Adeishvili, K.; Wüthrich, K. *Proc. Natl. Acad. Sci. U.S.A.* **2001**, *98*, 2358−2363.
(4) Fernández, C.; Hilty, C.; Wider, G.; Güntert, P.; Wüthrich, K. *J. Mol. Biol.* **2004**, *336*, 1211−1221.
(5) Hwang, P. M.; Choy, W. Y.; Lo, E. I.; Chen, L.; Forman-Kay, J. D.; Raetz, C. R.; Prive, G. G.; Bishop, R. E.; Kay, L. E. *Proc. Natl. Acad. Sci. U.S.A.* **2002**, *99*, 13560−13565.
(6) Pervushin, K.; Riek, R.; Wider, G.; Wüthrich, K. *Proc. Natl. Acad. Sci. U.S.A.* **1997**, *94*, 12366−12371.
(7) Oxenoid, K.; Kim, H. J.; Jacob, J.; Sönnichsen, F. D.; Sanders, C. R. *J. Am. Chem. Soc.* **2004**, *126*, 5048−5049.
(8) Kosen, P. A. *Methods Enzymol.* **1989**, *177*, 86−121.
(9) Hubbell, W. L.; Altenbach, C. *Curr. Opin. Struct. Biol.* **1994**, *4*, 566−573.
(10) Gaponenko, V.; Howarth, J. W.; Columbus, L.; Gasmi-Seabrook, G.; Yuan, J.; Hubbell, W. L.; Rosevear, P. R. *Protein Sci.* **2000**, *9*, 302−309.
(11) Battiste, J. L.; Wagner, G. *Biochemistry* **2000**, *39*, 5355−5365.
(12) Gillespie, J. R.; Shortle, D. *J. Mol. Biol.* **1997**, *268*, 158−169.
(13) Gillespie, J. R.; Shortle, D. *J. Mol. Biol.* **1997**, *268*, 170−184.

10.1021/ja0574825 CCC: $33.50

protein Mistic, which contains four α-helices.[14] In this work, PRE distance restraints were classified into four qualitative categories and were used in combination with medium- and a limited number of long-range NOE restraints to solve the structure of this protein.

The goal of the present work is to critically evaluate PRE as a general method to obtain long-range distance restraints for integral membrane proteins. In preliminary work, we found that nitroxide spin labels were often difficult to reduce completely in membrane-like environments and that incomplete reduction can lead to erroneous distances in membrane proteins. To avoid complications from incomplete reduction of the nitroxide spin labels, we introduce a new method of parallel labeling with paramagnetic and diamagnetic compounds of very similar structures to get more reliable measurements of the PRE effect in membrane proteins. We show that parallel SDSL and PRE can be employed to successfully refine membrane protein structures using the outer membrane protein A (OmpA) as an example. With a sufficient number of strategically placed nitroxides, it is even possible to obtain structures of reasonable quality from PRE distances only, in the absence of any NOEs.

Methods and Theory

Sample Preparation. The TM domain of wild-type OmpA has no cysteines, so single cysteine mutants of the OmpA TM domain were engineered using the QuikChange site-directed mutagenesis kit (Stratagene) on the plasmid that codes for the single tryptophan (Trp 7) mutant of OmpA.[2] For simplicity, we call this "wild-type" OmpA from here on. A total of 11 single cysteine mutants were made: 3 in the periplasmic turns (N46C, T88C, and T132C), 4 in the middle of the β-barrel (A11C, M53C, T95C, and L139C), and another 4 at the top of the barrel close to the extracellular loops (L35C, Q75C, V119C, and G160C) (Figure 1). For the mutants in the barrel, the mutation sites were selected so that their side-chains point toward the membrane.[2,15] Uniformly ^{2}H, ^{15}N labeled single cysteine OmpA proteins were overexpressed in the BL21(DE3)pLysS cells under the control of the T7 promoter by means of IPTG induction. Mutant proteins were extracted and purified in 8 M urea in their denatured states as previously described.[2] Purified proteins were concentrated to 1 mM, and a 20-fold molar excess of dithiothreitol (DTT) was added to ensure that the cysteines were kept in the reduced state. After 2 h of incubation, the protein solutions were run over a pre-equilibrated PD10 size exclusion column (Amersham Biosciences) to separate the proteins from DTT.

Purified reduced OmpA was split into two equal portions for parallel labeling with (1-oxyl-2,2,5,5-tetramethyl-η^3-pyrroline-3-methyl)methanethiosulfonate (MTSSL, Toronto Research Chemicals Inc.) and a diamagnetic analogue of MTSSL: (1-acetyl-2,2,5,5-tetramethyl-η^3-pyrroline-3-methyl)methanethiosulfonate (dMTSSL, Toronto Research Chemicals Inc.), in which the oxygen on the nitroxide of MTSSL was replaced with an acetyl group. Both reagents were added from 200 mM stocks in acetonitrile at a 10-fold molar excess over protein. To ensure complete labeling, another 10-fold excess of reagent was added after 30 min followed by a 2 h or overnight incubation at room temperature. Free labels were removed by gel-filtration on a PD10 column. Proteins were refolded in the presence of dodecylphosphocholine (DPC) micelles, concentrated, and the buffer was exchanged as described previously.[2] The final samples had protein concentrations ranging from 0.5 to 1.5 mM and a DPC concentration of approximately 600 mM. Samples for matrix-assisted laser desorption ionization mass spectroscopy (MALDI-MS) were prepared from the purified material before refolding by overnight dialysis to remove urea and salts and were analyzed on a PE Biosystems Voyager DE-Pro instrument. Typically, about 5 μL of 10 μM protein solutions were injected. The presence of small amounts of DPC (<5 mM) did not interfere with these measurements. Following conventions of the electron magnetic resonance (EPR) community, MTSSL-labeled side chains are denoted as R1, and dMTSSL-labeled side chains are denoted as R1′. For example, N46R1 and N46R1′ stand for paramagnetically and diamagnetically labeled N46C mutants, respectively, of the OmpA TM domain.

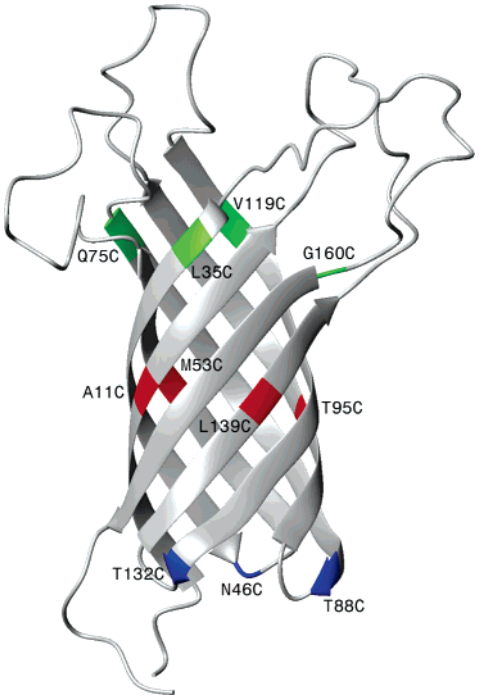

Figure 1. Ribbon representation of the solution structure of OmpA TM domain determined in DPC micelles by NMR (PDB code: 1G90). Residues selected for cysteine mutation and spin labeling are shown in color: "top-barrel" in green, "mid-barrel" in red, and "turn" mutants in blue. All protein structure figures were generated with the program MOLMOL.[24]

EPR Spectroscopy. Paramagnetically labeled samples were filled into glass capillaries for EPR spectroscopy. Spectra were recorded using a Varian E-line Centuries Series EPR spectrometer fitted with a microwave preamplifier and a two-loop, one-gap X-band resonator (Medical Advances, Milwaukee, WI). All spectra were recorded at room temperature and were typically an average of four 30 s scans over a field of 100 G.

NMR Spectroscopy and PRE Distances. TROSY-based ^{15}N−^{1}H heteronuclear single quantum coherence (HSQC) spectra were collected at 50 °C at 500 MHz ^{1}H frequency on a Varian Unity Inova 500 MHz NMR spectrometer, except for those of T132R1 and T132R1′ which were collected at 600 MHz on a Varian Unity Inova 600 MHz NMR spectrometer. Typically, 512 complex points in the direct dimension (^{1}H) and 96 complex points in the indirect dimension (^{15}N) were collected. Spectra were processed and analyzed with NMRPipe[16] and Sparky.[17] Peak assignments of spin-labeled OmpA mutants were based on comparison with wild-type OmpA spectra. Significant chemical shift changes were found for residues which were close to the mutation sites. In extreme cases where relatively large chemical shifts caused an overlap with neighboring peaks, we denoted affected peaks as unassigned, and such peaks were excluded from any further analysis.

PRE distances were determined from the 2D spectra by the method introduced by Battiste and Wagner.[11] The method makes use of the

(14) Roosild, T. P.; Greenwald, J.; Vega, M.; Castronovo, S.; Riek, R.; Choe, S. *Science* **2005**, *307*, 1317−1321.
(15) Pautsch, A.; Schulz, G. E. *Nat. Struct. Biol.* **1998**, *5*, 1013−1017.
(16) Delaglio, F.; Grzesiek, S.; Vuister, G. W.; Zhu, G.; Pfeifer, J.; Bax, A. *J. Biomol. NMR* **1995**, *6*, 277−293.
(17) Goddard, T. D.; Kneller, D. G. *SPARKY 3*; University of California: San Francisco, 2004.

modified Solomon−Bloembergen equation for transverse relaxation,[8,18]

$$r = \left[\frac{K}{R_2^{sp}}\left(4\tau_c + \frac{3\tau_c}{1+\omega_h^2\tau_c^2}\right)\right]^{1/6} \quad (1)$$

where r is the distance between the unpaired electron (approximately localized on the nitrogen atom of the nitroxide spin label) and the nuclear spins (the amide protons); K is a constant, 1.23×10^{-32} cm^6 s^{-2}; τ_c, the correlation time for the electron−nuclear interaction, is approximated as the global rotational correlation time of OmpA (20.7 ns);[19] ω_h is the Larmor frequency of the proton nuclear spin; and R_2^{sp} is the transverse relaxation rate enhancement contributed by the paramagnetic spin-label. A 10% error of τ_c translates into a 2% or approximately 0.2−0.4 Å error of the calculated distances. This is well within the error limits of the method (see Results) and, therefore, does not affect the structure calculations. Error limits of τ_c of up to 40% may be tolerated. R_2^{sp} is determined by

$$\frac{I_{para}}{I_{dia}} = \frac{R_2 \exp(-R_2^{sp} t)}{R_2 + R_2^{sp}} \quad (2)$$

where I_{para} and I_{dia} are peak heights of resonances in the MTSSL- and dMTSSL-labeled protein spectra, respectively; R_2 is the transverse relaxation rate of the resonance in the diamagnetic sample, which was estimated from the half-height line widths assuming Lorentzian line shapes; t is the total evolution time in the proton dimension (11.8 ms). To account for possible small fluctuations of the spectrometer response and small differences in protein concentration, we calibrated raw peak heights by using at least six unperturbed (>26 Å distance) resonance peaks.

Molecular Modeling. To determine R1 and R1′ side chain conformations, 12 distances were randomly picked from the PRE distances that were determined from the measured intensity ratios (I_{para}/I_{dia}) and were modeled into the high-resolution X-ray structure (PDB code: 1QJP)[20] using the program InsightII (Biosym Technologies, San Diego) with the CVFF force field. The accuracy of the measured intensity ratios is best in the range from 15 to 85%; therefore, only ratios in this range were used for the modeling. All experimental distances were used with ±2 Å upper/lower bounds in these modeling studies, in which all atoms were kept fixed except for those of the R1 side chain, whose most likely conformation was determined by this procedure.

Structure Calculations. Two sets of restraints were incorporated into the structure calculations: (a) for protons with I_{para}/I_{dia} ratios between 15 and 85%, calculated distances were incorporated with ±2 Å upper/lower bounds; and (b) for protons whose I_{para}/I_{dia} ratios were less than 15%, including protons whose resonances were no longer observable in the paramagnetic spectra, an upper distance limit of 15 Å was employed. Protons with I_{para}/I_{dia} ratios > 85% were considered unrestrained. Separate calculations were performed for comparison with the upper/lower bounds set at ±3 Å and an upper distance limit of 16 Å. No large differences in overall violation energies were observed between these two sets of calculations.

The nitroxide side chains were built from ab initio calculations using Gaussian 98.[21] Structures of OmpA were calculated using the CNS v. 1.1[22] on an Aspen Linux cluster. PRE distances were added to the distance restraint files and included in the structure calculations in the same manner as NOE distances. A total of 90 NOE distances, 142 backbone dihedral angles, and 136 hydrogen bond restraints were taken from previous work.[2] To utilize PRE restraints from multiple mutants, energy minimization and annealing were performed on virtual OmpA molecules with simultaneously incorporated multiple nitroxide side chains. In all calculations, 4000 steps of high-temperature annealing, 8000 steps of torsion angle slow-cooling annealing, and 8000 steps of Cartesian slow-cooling annealing were used. Ten structures with the lowest overall violation energies were selected for the final representation of each calculation.

Results and Discussion

Strategy of Parallel Spin Labeling. It has been shown previously by EPR[23] and NMR[11] spectroscopy that appropriately placed nitroxide spin labels typically perturb structures of soluble proteins only minimally, predominantly in the spatial vicinity of the label. To minimize possible interference of the spin labels with the structure of OmpA, we selected sites for cysteine mutation and labeling so that the spin labels would face the membrane. Some resonances of residues around the R1 and R1′ sites exhibited relatively large changes in chemical shifts, whereas resonances of all other residues exhibited only very small chemical shift changes of less than 0.1/0.5 ppm in the ^{1}H/^{15}N dimensions. These results are similar to those in a previous report[11] in which the authors also concluded that the protein fold was not significantly perturbed by the introduction of R1 side chains. There were essentially no chemical shift differences of observable peaks between R1 and corresponding R1′ modified proteins even for residues that are close to the labeled sites, consistent with the very similar structures of the two labels.

To obtain accurate distances from PRE, it is important to ensure the labeling efficiency be as close to 100% as possible because any fraction of unlabeled protein would cause apparent reductions of the magnitude of the PRE effect. In most previous studies in which SDSL was used to measure PREs, proteins were labeled with only paramagnetic nitroxide spin labels. After the measurements of the paramagnetically labeled samples were completed, a reducing reagent such as ascorbic acid was typically added to reduce the nitroxide. This reduced diamagnetic sample was then measured to retrieve the intrinsic (unperturbed) relaxation rates of affected and unaffected protons. We tried this approach under many different conditions, including different values of pH, temperature, and incubation time. However, we were unable to completely reduce our membrane protein samples. As judged from their EPR spectra, residual paramagnetic species persisted in all these samples. For example, with T88R1, we achieved at best a ∼90% elimination of the paramagnetic species with a 10-fold molar excess of ascorbic acid over the protein. We also tried to reduce OmpA in the unfolded state and with different reducing agents, such as sodium dithionite, but without any improvement. Although we did not try to reduce any of the barrel mutants with these methods, it is likely that the apolar environment of the surrounding lipids makes this reduction even more difficult.

To circumvent the problem of incomplete reduction of MTSSL-labeled samples, we adopted the strategy of parallel labeling. The diamagnetic analogue dMTSSL was coupled to the protein in parallel and in exactly the same manner as MTSSL. To ensure efficient labeling, we coupled MTSSL and

(18) Solomon, I.; Bloembergen, N. *J. Chem. Phys.* **1956**, *25*, 261−266.
(19) Tamm, L. K.; Abildgaard, F.; Arora, A.; Blad, H.; Bushweller, J. H. *FEBS Lett.* **2003**, *555*, 139−143.
(20) Pautsch, A.; Schulz, G. E. *J. Mol. Biol.* **2000**, *298*, 273−282.
(21) Frisch, M. J.; et al. *Gaussian 98*, revision A.6; Gaussian, Inc.: Pittsburgh, PA, 1998.
(22) Brunger, A. T.; Adams, P. D.; Clore, G. M.; Delano, W. L.; Gros, P.; Grosse-Kunstleve, R. W.; Jiang, J.-S.; Kuszewski, J.; Nilges, M.; Pannu, N. S.; Read, R. J.; Rice, L. M.; Simonson, T.; Warren, G. L. *Acta Crystallogr., Sect. D: Biol. Crystallogr.* **1998**, *54*, 905−921.
(23) Mchaourab, H. S.; Lietzow, M. A.; Hideg, K.; Hubbell, W. L. *Biochemistry* **1996**, *35*, 7692−7704.

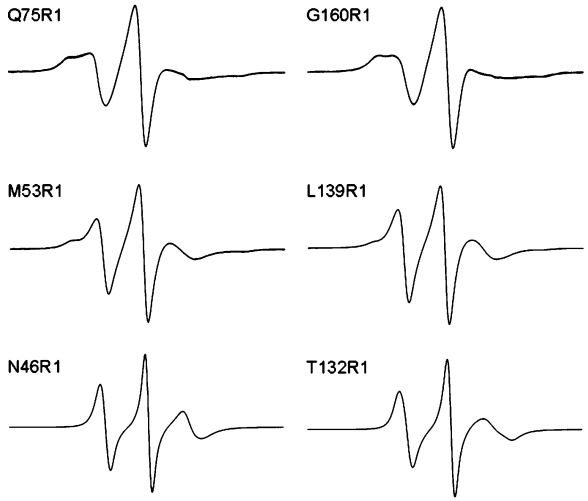

Figure 2. X-band EPR spectra of MTSSL-labeled single cysteine mutants of OmpA. The spectra in the top row are those of "top-barrel", in the middle row are those of "mid-barrel", and at the bottom are those of "turn" mutants. The magnetic field scan width is 100 G in all spectra.

dMTSSL to OmpA in the denatured state. This method ensured that labeling efficiencies were close to unity for both reagents and at every site, as verified by MALDI-MS and EPR. Mass spectra of MTSSL-, dMTSSL-, and unlabeled samples showed only single major peaks with peak values corresponding to the expected masses of the labeled and unlabeled proteins, respectively. EPR spectra of the MTSSL-labeled proteins are shown in Figure 2. Spin concentrations were measured from the EPR spectral intensities, which were obtained by double integration of the single derivative spectra shown in Figure 2. The ratios between spin and protein concentrations, which were measured by UV absorption at 280 nm, were always close to unity, confirming a high degree of labeling. In addition, TROSY−HSQC spectra showed no traces of additional peaks in any of the labeled samples. Finally, T_1 and T_2 relaxation times were measured for some of our samples. All peaks showed single exponential decays, indicative of a single species.

NMR Spectroscopy and PRE Distances. Figure 3 shows TROSY-based $^{15}N-^{1}H$ HSQC spectra of two selected mutants, N46C and G160C, that were labeled with dMTSSL (top) or MTSSL (middle). The positions of these residues are shown in green in the ribbon diagrams of the structures at the bottom. The patterns of affected peaks in the spectra and the corresponding residues in the structures (both shown in red in Figure 3) clearly show that PRE is distance-dependent. To quantify the effects of PREs, we measured peak heights and line widths and calculated distances following the method of Battiste and Wagner,[11] as briefly described in the "Methods and Theory" section. Although peak-fitting routines could, in principle, be used to measure intensities of individual resonances, we found that these procedures introduced errors because of imperfections in the line shapes and problems with even only marginally overlapped peaks with distorted line shapes. More severely overlapped peaks were completely omitted from our analysis because peak heights are not good representations of intensities in these cases and because the assignments of such peaks were more ambiguous.

To examine whether intermolecular relaxation could contribute to a reduction of peak intensities, measurements were carried out as a function of OmpA concentration. The intensity ratios were unaffected within the examined and experimentally accessible concentration range of 0.3−2 mM. This is not surprising because the presence of the lipid molecules likely prevents intermolecular interactions and direct contacts between the membrane portions of the protein−lipid complexes.

A distance vs intensity ratio curve was generated from eqs 1 and 2 under the assumption that τ_c equals the global correlation time and R_2 is deduced from the average half-height line width (data not shown). This curve was very similar to the one shown in Figure 3C of ref 11. Therefore, reconfirming the conclusions of these previous authors, we also find that distances determined from peak intensity ratios (I_{para}/I_{dia}) between 15 and 85% can be used as reliable distance restraints in structure calculations.

To further evaluate the quality and reliability of the data and to estimate an error range of distances determined by PRE, we modeled these distances into the high-resolution crystal structure of the OmpA TM domain (1QJP).[20] Using 12 randomly selected distances with ±2 Å upper/lower bounds for each of the seven spin labels on the periplasmic turns and in the middle of the β-barrel, the conformations of the spin-labeled side chains were modeled into the fixed backbone of the crystal structure. We did not include the four residues that are close to the extracellular loops in these modeling studies because the solution and crystal structures show significant differences in this region. However, they agree very well in the barrel center and periplasmic turn regions. Figure 4 shows a graph of the best-fit modeled distances vs the PRE-derived experimental distances. In this figure, all distances that could be calculated, i.e., all that have $I_{para}/I_{dia} < 1$, are included.

A closer inspection of Figure 4 reveals two striking features. First, the correlation between calculated distances and experimental distances is very good in the range between 15 and 24 Å. This range roughly corresponds to I_{para}/I_{dia} ratios between 15 and 85%. The correlation degrades rapidly for distances greater than 24 Å. Three PRE distances were calculated from I_{para}/I_{dia} ratios less than 15%. These distances were around 14 Å but fell below the −2 Å lower bound when correlated with the calculated structures. Because, in addition, approximately twenty peaks were totally eliminated in the MTSSL-labeled samples, we again conclude that the experimentally measurable range of PRE distances begins at 15 Å. Therefore, it is reasonable to set an upper limit of 15 Å in structure calculations for all residues with I_{para}/I_{dia} ratios less than 15%. A second remarkable feature of Figure 4 is that the upper/lower bounds of ±2 Å represent very well the experimental error ranges for the calculated PRE distances. We determined a total of 178 PRE distances from I_{para}/I_{dia} ratios between 15 and 85%, but only 12 distances from each of the 7 paramagnetic centers were included in these molecular modeling tests. Most modeled distances in the 15−24 Å range are within the ±2 Å upper/lower bounds (broken lines), and evenly distributed around the diagonal. The few data points outside these bounds were distances from spin labels to residues on the extracellular loops, the C-terminus, or on the very top of the barrel where differences between the crystal and the solution structure are most significant. In fact, the majority of these discrepancies are at the extracellular end of the fifth β-strand and the directly adjacent third extracellular loop. In this context, to stabilize the crystal contacts, a mutation (Lys107 → Tyr) was introduced in this same third loop.[15,20] It

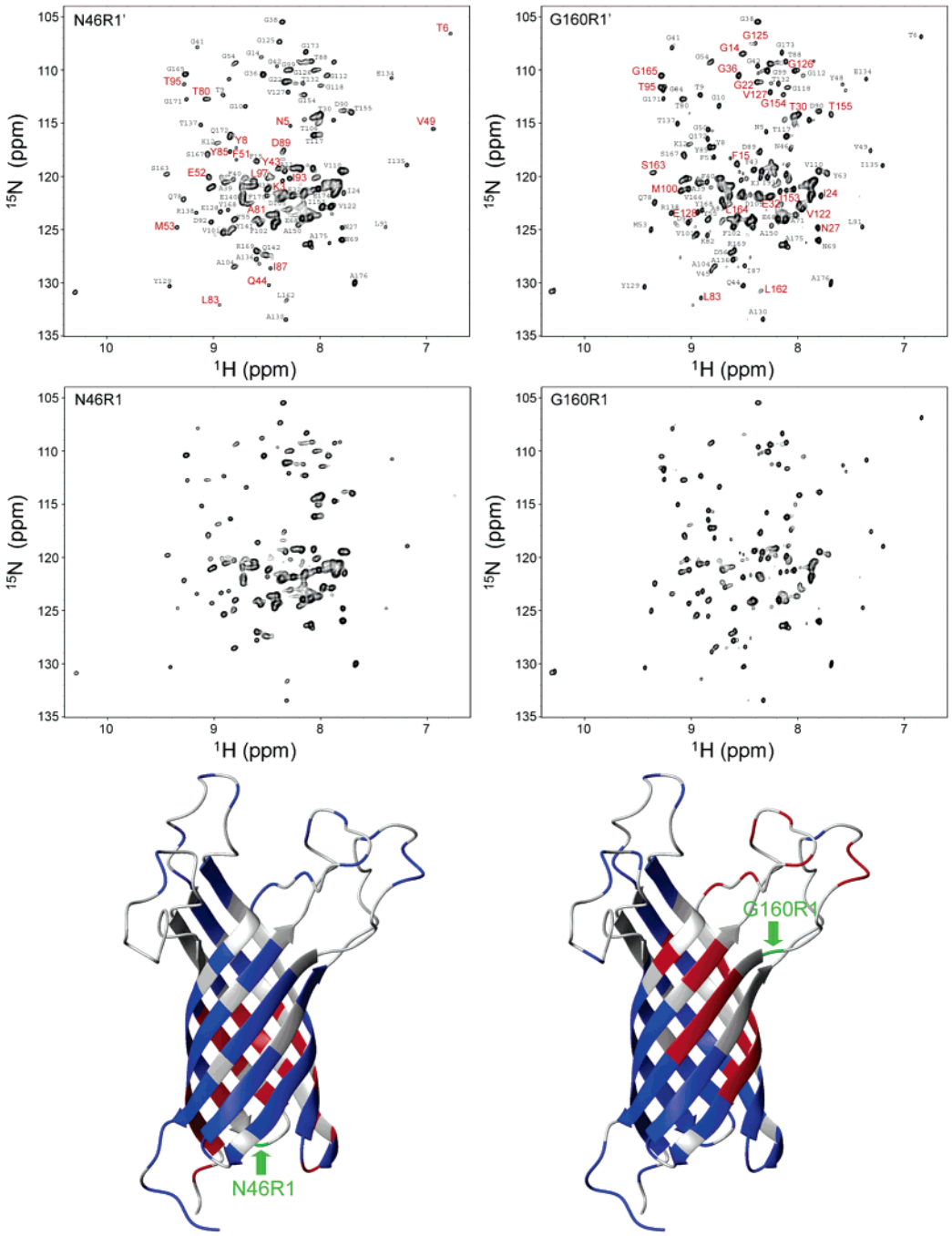

Figure 3. TROSY-based HSQC spectra of single cysteine mutants of OmpA labeled with dMTSSL (top) and MTSSL (middle) measured at 500 MHz ^{1}H frequency. Resonances with I_{para}/I_{dia} ratios less than 70% are labeled in red. Bottom: ribbon representations of color-coded OmpA structures. The sites of mutated cysteines are denoted with green arrows and labels, residues with I_{para}/I_{dia} ratios less than 70% are shown in red (corresponding to red peaks in corresponding spectra on the top), and unassigned or unresolved residues are shown in gray. All other residues are shown in blue.

is therefore not surprising that the crystal and solution structures diverge most in this region.

Structure Calculations. PRE distances were incorporated into structure calculations as described in the "Methods and Theory" section. Structure calculations were first performed using three different sets of PRE distance restraints plus all other available "regular" restraints (NOEs, hydrogen bonds, and dihedral angles). These three sets of PRE distances were grouped on the basis of the locations of spin labels on the structure of OmpA to separately evaluate the effects of each set on the structure calculations. Mutants N46R1, T88R1, and T132R1 are "turn" mutants, A11R1, M53R1, T95R1, and L139R1 are "mid-barrel" mutants, and L35R1, Q75R1, V119R1, and G160R1 are "top-barrel" mutants. Backbone rmsd's of the 10 lowest violation energy conformers were calculated for each of these sets with their respective PRE restraints. To compare the effects of the PRE's on different parts of the structure, rmsd's were further subgrouped into β-strand, core, and core plus turn residues. β-strand residues were defined in the same way as in ref 2 (see also footnote c in Table 1), core residues were a subset of the β-strand residues, namely those that form a closed β-barrel and are within the boundary of the lipid bilayer (footnote d in Table 1), and core + turn residues were the core residues plus residues on the three periplasmic turns (footnote e in Table 1). The results

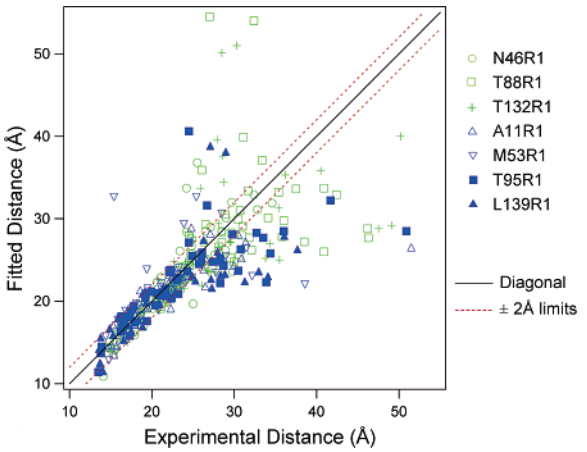

Figure 4. Best-fitted distances from models of spin labels modeled onto the crystal structure of OmpA (1QJP) vs experimental distances determined from the PRE measurements. Data from three turn (green symbols) and four mid-barrel (blue symbols) mutant sites are included.

of these calculations are listed in Table 1 with the spin-label sets organized in columns and rmsd structure groups organized in rows. These data clearly show that both precision (comparison of structures among themselves) and accuracy (comparison of NMR structures with high-resolution crystal structure) of the calculated structures are significantly improved upon the addition of PRE restraints. In particular, the PRE restraints from the "turn" spin-labels improved the structures of the core and turn residues quite dramatically in both precision (from 1.25 ± 0.29 to 0.87 ± 0.12 Å) and accuracy (from 1.62 ± 0.16 to 1.35 ± 0.10 Å). Finally, the structure calculation was performed by simultaneously using all PRE restraints. The precision of the core and turn residues of the 10 lowest conformers is 0.85 ± 0.17 Å, and the accuracy is 1.09 ± 0.12 Å. A comparison of the ensemble of structures calculated with and without the full set of 320 PRE restraints is shown in Figure 5.

The top-barrel spin labels improved the structures of the barrel and core residues to a similar degree as the turn spin labels. However, they only marginally improved the structures of the turns. This is expected because the turns are more than 25 Å away from the top-barrel spin labels. The PRE restraints from the mid-barrel mutants also improved the structures but not significantly more than those from the turn restraints. This is somewhat surprising because the centrally located mid-barrel mutants add the highest number of PRE restraints to the structure calculations. However, some of these "extra" PRE restraints may be redundant and, hence, may not improve the structures, because the structure is already highly defined in this region by a number of strong hydrogen bond restraints. To test this hypothesis, we carried out structure calculations in the absence of hydrogen-bond restraints. The results of these calculations are summarized in Table 2, and corresponding ensemble structures are shown in Figure 6. The global fold of OmpA is very poorly defined in the absence of both hydrogen bond and PRE restraints. Even though the barrel did fold due to long-range HN−HN NOEs between neighboring β-strands, the handedness of the β-barrrel was not defined. Among 10 lowest-energy conformers, 2 had incorrect overall folds. Viewed from the extracellular side to the periplasmic side, the correct β-barrel has a clockwise arrangement of strands β1 to β8, whereas the incorrect barrel has a counterclockwise arrangement. When the different sets of PRE restraints were added, the problem could not be corrected with the "turn" or "top-barrel" restraints alone. By contrast, the addition of the "mid-barrel" PRE restraints was necessary and sufficient to define the correct handedness of the structure.

The rmsd values listed in Table 2 also show a gradual improvement of the calculated OmpA structures depending on which set(s) of PRE distance restraints were added. When the structure was calculated in the absence of hydrogen-bond restraints, but in the presence of the full set of PRE distance restraints, the overall improvement was significant: the rmsd value of the 10 lowest conformers for the core + turn residues was 1.24 ± 0.12, and the accuracy was 1.63 ± 0.08. The same precision and accuracy values for the 10 lowest conformers calculated from hydrogen-bond restraints without PRE (Table 1, last column) were 1.25 ± 0.29 and 1.62 ± 0.16. This shows that experimental PRE restraints are able to fully substitute artificially introduced predicted hydrogen bond restraints. We also examined whether an introduction of lower limits for residues that show $I_{para}/I_{dia} > 85\%$ would further improve the quality of the calculated structures. We recalculated the data of Table 2 with 340 lower limit restraints of 22 and 20 Å for this class of residues. The rmsd's calculated with 22 Å lower limits were marginally (~0.06 Å) improved, which is still within the given error limits of Table 2. Lower limits of 20 Å did not improve the structures at all. Therefore, we recommend not using lower limits for this class of residues in structure calculations with PRE's.

The introduction of PRE restraints also improved the identification of the secondary structure in the solution structure of OmpA with the program MOLMOL.[24] The average structure of the 10 lowest conformers from the calculation with PRE identified a total of 60 residues to be in β-strands, whereas only 18 β-strand residues were identified in the average structure from the calculation without PRE restraints. The numbers of β-sheet residues in the crystal structure[15] and the average NMR structure calculated with hydrogen bond restraints[2] were 102 and 81, respectively. Long β-strands were clearly present in the PRE structure, but they were shorter (3, 5, 2, 2, 2, 5, 1, and 1 residues shorter for 8 β-strands) than in the hydrogen bond structure. Four strands (β1, β4, β5, and β8) had breaks in the middle in the PRE but not in the hydrogen bond structure.

To simulate a situation that is often encountered with helical membrane proteins, in which the number of long-range NOEs is often severely limited, we took an extreme approach and eliminated all NOE distance restraints from our structure calculations. (All hydrogen bond restraints were also removed because they are a special feature of β-barrels and very few or no such long-range restraints are expected in helical membrane proteins.) The 10 lowest violation energy conformers calculated from 320 PRE distances and 142 dihedral angle restraints only were still folded into the correct β-barrel conformation (Figure 6c). The backbone rmsd value calculated from this ensemble of conformers (Table 3, fourth column) also was improved over those from structures that were calculated from NOE distances and dihedral angle restraints only (Figure 6a; Table 2, last column). This average structure had a total of 42 β-strand residues, and the shortest β-strand was only three residues long. Clearly 320 PRE restraints produce better structures than 90 NOE restraints, although PRE distances are less precise than

(24) Koradi, R.; Billeter, M.; Wüthrich, K. *J. Mol. Graphics* **1996**, *14*, 51−55.

Table 1. Backbone rmsd Statistics of Structures Calculated with Different Groups of PRE Distance Restraints and Regular (NOE, Hydrogen Bond, Dihedral Angle) Restraints

	turn[f]	top-barrel[g]	mid-barrel[h]	all PRE[i]	without PRE
β-strand[a,c]	0.98 ± 0.17	0.95 ± 0.18	0.86 ± 0.15	0.78 ± 0.11	1.18 ± 0.24
core[a,d]	0.71 ± 0.10	0.80 ± 0.16	0.73 ± 0.14	0.67 ± 0.11	1.01 ± 0.27
core + turn[a,e]	0.87 ± 0.12	1.13 ± 0.19	1.02 ± 0.17	0.85 ± 0.17	1.25 ± 0.29
β-strand[b,c]	2.14 ± 0.20	1.60 ± 0.21	1.82 ± 0.17	1.61 ± 0.07	2.22 ± 0.24
core[b,d]	1.27 ± 0.10	1.05 ± 0.11	1.09 ± 0.07	0.97 ± 0.07	1.32 ± 0.15
core + turn[b,e]	1.35 ± 0.10	1.40 ± 0.19	1.37 ± 0.08	1.09 ± 0.12	1.62 ± 0.16

[a] Precision: rmsd of 10 lowest overall violation energy conformers. [b] Accuracy: rmsd of 10 lowest overall violation energy conformers compared with the high-resolution crystal structure (1QJP). [c] β-strand residues: 6−16, 34−44, 49−55, 75−86, 91−103, 118−130, 135−142, 161−169. [d] Core residues: 6−14, 36−44, 49−55, 77−86, 91−99, 122−130, 135−142, 162−169. [e] Core + turn residues: 6−14, 36−55, 77−99, 122−142, 162−169. [f] The number of PRE restraints with ±2 Å upper/lower bounds is 73 and with upper bounds (<15 Å) is 13. [g] The number of PRE restraints with ±2 Å upper/lower bounds is 83 and with upper bounds (<15 Å) is 14. [h] The number of PRE restraints with ±2 Å upper/lower bounds is 103 and with upper bounds (<15 Å) is 34. [i] The number of PRE restraints with ±2 Å upper/lower bounds is 259 and with upper bounds (<15 Å) is 61.

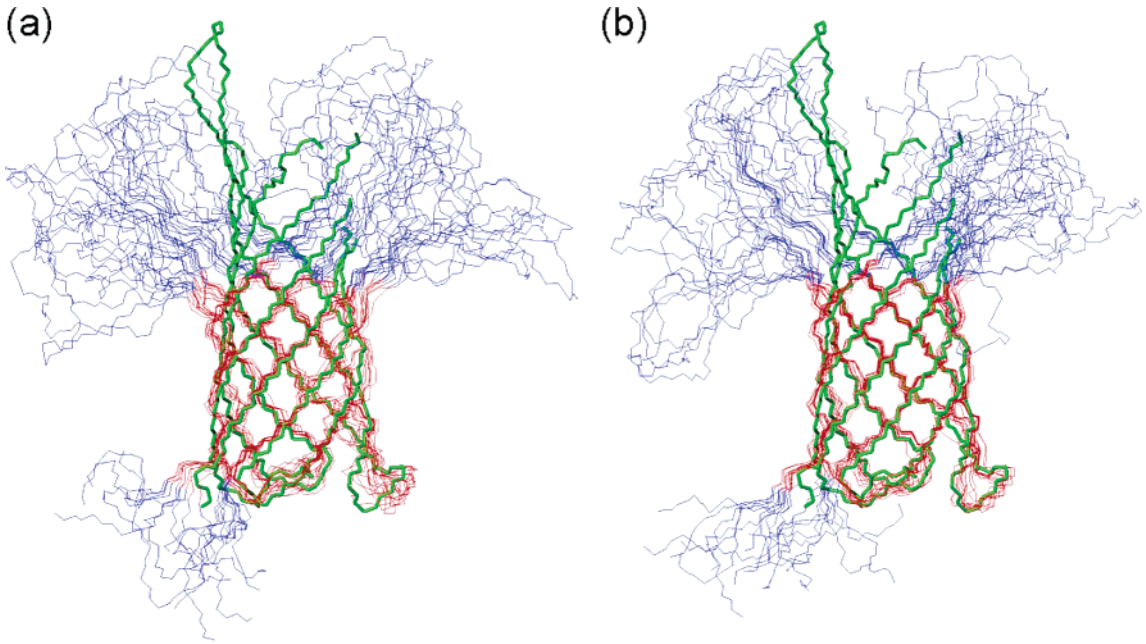

Figure 5. Superpositions of 10 lowest violation energy conformers calculated (a) without PRE restraints, (b) with 320 PRE restraints, in addition to 90 NOE distances, 142 dihedral angles, and 136 hydrogen-bond restraints. Residues used for overlay are in red (the "core + turn" residues as defined in Table 1). For comparison, the crystal structure (1QJP) is shown in green.

Table 2. Backbone rmsd Statistics of Structures Calculated with Directly Observed Distance (NOE, PRE, but No Hydrogen Bond) and Angle Restraints

	turn[d]	top-barrel[d]	mid-barrel[e]	all PRE[e]	without PRE[d]
β-barrel[a]	no	no	yes	yes	no
β-strand[b]	1.90 ± 0.32	1.77 ± 0.31	1.66 ± 0.21	1.44 ± 0.17	2.05 ± 0.38
core[b]	1.34 ± 0.16	1.54 ± 0.30	1.39 ± 0.23	1.09 ± 0.12	1.63 ± 0.30
core + turn[b]	1.46 ± 0.21	1.94 ± 0.39	1.69 ± 0.41	1.24 ± 0.12	1.99 ± 0.37
β-strand[c]	3.02 ± 0.32	3.03 ± 0.30	2.51 ± 0.20	2.40 ± 0.25	3.49 ± 0.22
core[c]	2.14 ± 0.14	2.19 ± 0.21	1.73 ± 0.11	1.47 ± 0.08	2.46 ± 0.19
core + turn[c]	2.37 ± 0.17	2.82 ± 0.22	2.17 ± 0.21	1.63 ± 0.08	3.06 ± 0.26

[a] Structures formed with the correct handedness of the β-barrel. [b] Precision, definitions of β-strand, core, and core + turn residues as in Table 1. [c] Accuracy, definitions of β-strand, core, and core + turn residues as in Table 1. [d] Rmsd values of 10 lowest overall violation energy conformers. Only conformers whose β-strands form the correct barrel were selected. [e] Rmsd values of 10 lowest overall violation energy conformers.

NOE distances. The larger number and the longer distance range of PREs compensate for the better precision of the NOEs.

Finally, structure calculations were performed using less restrictive bounds for the PRE distances. Upper/lower bounds of ±3 Å were used for residues with I_{para}/I_{dia} ratios between 15 and 85%, and an upper limit of 16 Å was used for residues with I_{para}/I_{dia} ratios smaller than 15%. As expected, the 10 conformers calculated with the ±3 Å bounds had larger rmsd values than those calculated with ±2 Å bounds (Table 3). Importantly, the accuracies of these structures decreased concurrently with their precisions. This result justifies our choice of the selected error range of ±2 Å. The ±2 Å bounds with a 15 Å cutoff is adequate and sufficient for structure calculations with a sufficient number of PRE distances.

Flexible Loop Residues. We deliberately did not include any PRE distance restraints for residues in the four extracellular loops, as these loops show increased mobility relative to the remainder of the protein;[19] thus, the use of the global correlation time in calculations for these residues would not be appropriate. To get accurate distances, individual correlation times would

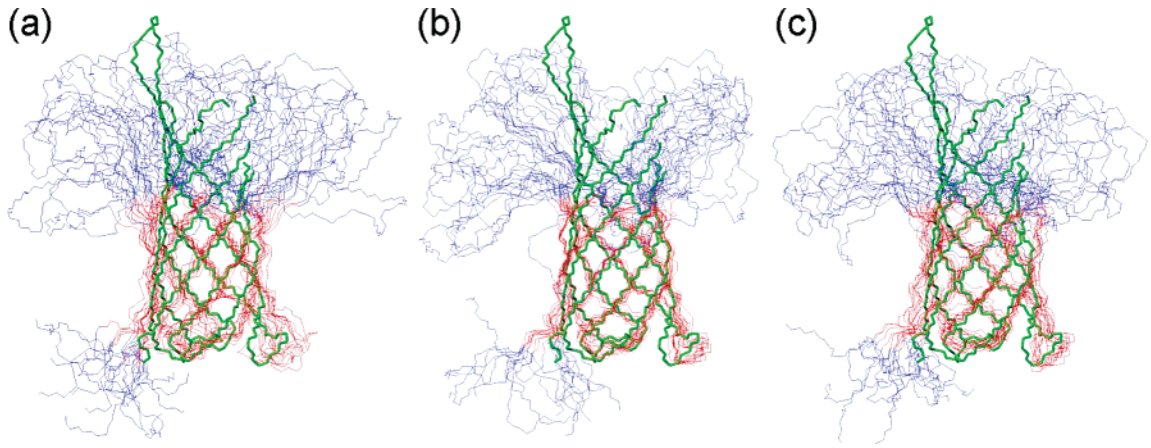

Figure 6. Superpositions of 10 lowest violation energy conformers calculated (a) with 90 NOE restraints, (b) with 90 NOE and 320 PRE restraints, and (c) with 320 PRE restraints, in addition to 142 dihedral angle restraints. Residues used for overlay are in red (the "core + turn" residues as defined in Table 1). For comparison, the crystal structure (1QJP) is shown in green. In (a), 10 conformers that formed barrels with the correct handedness were manually selected from the 13 lowest violation energy conformers.

Table 3. Backbone rmsd Statistics of 10 Lowest Violation Energy Conformers Calculated with PRE Distance Restraints in Combination with Other Types of Distance Restraints

	±2 Å upper/lower bounds			±3 Å upper/lower bounds[a]		
	PRE NOE H-bond	PRE NOE	PRE	PRE NOE H-bond	PRE NOE	PRE
β-strand[b]	0.78 ± 0.11	1.44 ± 0.17	2.10 ± 0.23	0.87 ± 0.13	1.65 ± 0.29	3.46 ± 0.52
core[b]	0.67 ± 0.11	1.09 ± 0.12	1.67 ± 0.22	0.73 ± 0.10	1.39 ± 0.21	3.06 ± 0.50
core + turn[b]	0.85 ± 0.17	1.24 ± 0.12	1.78 ± 0.29	0.89 ± 0.12	1.59 ± 0.25	3.26 ± 0.53
β-strand[c]	1.61 ± 0.07	2.40 ± 0.25	3.39 ± 0.22	1.70 ± 0.14	2.64 ± 0.13	4.01 ± 0.39
core[c]	0.97 ± 0.07	1.47 ± 0.08	2.18 ± 0.21	1.09 ± 0.11	1.71 ± 0.18	3.17 ± 0.34
core + turn[c]	1.09 ± 0.12	1.63 ± 0.08	2.31 ± 0.26	1.26 ± 0.08	1.96 ± 0.16	3.41 ± 0.40

[a] Also used 16 Å as the upper limit for residues with I_{para}/I_{dia} values less than 15%. [b] Precision, definitions of β-strand, core, and core + turn residues as in Table 1. [c] Accuracy, definitions of β-strand, core, and core + turn residues as in Table 1.

have to be determined for the loop residues. A more serious problem of the flexible nature of the loop residues is that the observed distance is not the average but the "closest contact" distance.[25,26] The effect of the r^{-6} distance dependence of PREs weighs shorter distances much more heavily than longer distances, which leads to distorted structures if the PRE distances of flexible regions are taken as average distances in the structure calculations. A sophisticated ensemble approach may be required to extract PRE distances for residues of this type.[27]

Dynamics and Other Considerations. PRE distance restraints in the current study were determined from relative intensities. Thus, our measurements are based on a T_2 relaxation effect. We also explored the possibility of determining PRE distance restraints based on T_1 relaxation. However, this approach did not yield satisfactory results due to a greater dependence of T_1 on internal motion. This has also been demonstrated in an earlier report.[27] An alternative to measuring intensities would be to directly measure T_2 relaxation times of diamagnetic and paramagnetic samples and to extract the PREs from a comparison of the measured T_2's. This potentially could improve the accuracy of the PRE distances, but it would require a much larger amount of spectrometer time.

An interesting issue is whether the dynamics of the spin label itself contributes to the experimentally determined distance restraints. For example, if the R1 side chain adopts two distinct conformations, the PRE distance will reflect mostly the shorter distance because of the r^{-6} average. Structures calculated with such distances will be distorted if multiple R1 conformations are not taken into account. However, this problem has been discussed quite extensively in the EPR community. The R1 side chain has relatively few allowed conformations. Among five possible dihedral angles extending from C_α on the protein backbone to C_ζ on the nitroxide ring, the first three are fixed and only the last two dihedral angles dictate the motion of the spin label.[28] This limited motional freedom of the nitroxide allows one to analyze the backbone dynamics of proteins from EPR line shapes in quite some detail.[29] The EPR spectra of the 11 sites of this study exhibited different line shapes reflecting different backbone motions (Figure 2). The backbone motions of the "mid-barrel" and "top-barrel" sites are limited, as revealed by the broader intrinsic line shapes of these spectra. By contrast, the spectra of "turn" sites are narrower, indicating more flexibility of the backbone around the periplasmic turns. Even with considerable local backbone motions, the local motion of the spin label itself is probably small, and the problem of the r^{-6} averaging is probably not serious. A potential further improvement and reduction of residual internal spin label

(25) North, C. L.; Franklin, J. C.; Bryant, R. G.; Cafiso, D. S. *Biophys. J.* **1994**, *67*, 1861−1866.
(26) Shenkarev, Z. O.; Paramonov, A. S.; Balashova, T. A.; Yakimenko, Z. A.; Baru, M. B.; Mustaeva, L. G.; Raap, J.; Ovchinnikova, T. V.; Arseniev, A. S. *Biochem. Biophys. Res. Commun.* **2004**, *325*, 1099−1105.
(27) Iwahara, J.; Schwieters, C. D.; Clore, G. M. *J. Am. Chem. Soc.* **2004**, *126*, 5879−5896.
(28) Langen, R.; Oh, K. J.; Cascio, D.; Hubbell, W. L. *Biochemistry* **2000**, *39*, 8396−8405.
(29) Columbus, L.; Hubbell, W. L. *Trends Biochem. Sci.* **2002**, *27*, 288−295.

motions would be to use a modified MTSSL spin-label with a bulky group attached to the C_η on the nitroxide ring to restrict its rotational freedom.[30] This measure would still not suppress effects of local backbone motions, but fortunately, the PRE distance calculations are relatively insensitive to local correlation time motions. Even with small amplitude local backbone motions present, the distances determined from the measured PREs should still accurately represent the actual distances between nitroxides and individual protons within the given experimental errors.

Concluding Remarks

In conclusion, parallel SDSL and PRE can provide valuable long-range distances to improve structure calculations of membrane proteins, as shown here for the case of OmpA. Even with limited data obtained from 2D $^{15}N-^{1}H$ TROSY-based HSQC spectra on a 500 MHz spectrometer, we have been able to significantly improve the solution structure of OmpA. PRE distance restraints are sufficient to define the correct β-barrel conformation of OmpA even in the absence of NOE and hydrogen-bond restraints. The use of parallel paramagnetic and diamagnetic labeling overcomes serious problems of incomplete reduction of spin-labeled proteins. This is particularly important for membrane proteins, which are harder to access with reducing reagents than soluble proteins because of the overall larger hydrophobicity and the protection by lipids in the lipid/protein micelle complexes. Although the β-barrel membrane protein OmpA has been used as a model in the current study, the method of parallel SDSL and PRE should be of even greater use for α-helical membrane proteins, where long-range hydrogen bond and NOE restraints are virtually absent. Indeed, parallel spin labeling and PRE may be the best way to obtain sufficient restraints to determine the folds of helical bundle membrane proteins by solution NMR.

Acknowledgment. This work was supported by NIH Grants R01 GM051329 (to L.K.T.) and GM R21 GM070825 (to J.H.B.). We thank Dr. Ashish Arora (currently CDRI, Lucknow, India) for some preliminary experiments in this project.

Supporting Information Available: Complete ref 21. This material is available free of charge via the Internet at http://pubs.acs.org.

JA0574825

(30) Columbus, L.; Klai, T.; Jek, J.; Hideg, K.; Hubbell, W. L. *Biochemistry* **2001**, *40*, 3828−3846.